Naval Research Laboratory

Washington, DC 20375-5320

NRL/MR/6170--20-10,182

In Situ Tribocorrosion: Uncovering the Science Behind Coupled Surface Damage Processes

Kathryn J. Wahl

Christopher R. So

Christopher N. Chervin

Surface Chemistry Branch
Chemistry Division

Derek J. Horton

Steven Policastro

Matthew Strom

Mary E. Parker

Center for Corrosion Science and Engineering Branch
Chemistry Division

November 3, 2020

REPORT DOCUMENTATION PAGE

Form Approved
OMB No. 0704-0188

1. REPORT DATE *(DD-MM-YYYY)*	**2. REPORT TYPE**	**3. DATES COVERED** *(From - To)*
00-00-2020	NRL Memorandum Report	1 Oct 16 – 30 Sep 20

4. TITLE AND SUBTITLE

In Situ Tribocorrosion: Uncovering the Science Behind Coupled Surface Damage Processes

5a. CONTRACT NUMBER

5b. GRANT NUMBER

5c. PROGRAM ELEMENT NUMBER
61553N

6. AUTHOR(S)

Kathryn J. Wahl, Derek J. Horton, Steven Policastro, Matthew Strom, Christopher R. So, Christopher N. Chervin, and Mary E. Parker

5d. PROJECT NUMBER

5e. TASK NUMBER

5f. WORK UNIT NUMBER
1E19

7. PERFORMING ORGANIZATION NAME(S) AND ADDRESS(ES)

Naval Research Laboratory
4555 Overlook Avenue, SW
Washington, DC 20375-5320

8. PERFORMING ORGANIZATION REPORT NUMBER

NRL/MR/6170--20-10,182

9. SPONSORING / MONITORING AGENCY NAME(S) AND ADDRESS(ES)

Office of Naval Research
One Liberty Plaza
875 N Randolph Street
Arlington, VA 22217-1995

10. SPONSOR / MONITOR'S ACRONYM(S)
ONR

11. SPONSOR / MONITOR'S REPORT NUMBER(S)

12. DISTRIBUTION / AVAILABILITY STATEMENT

DISTRIBUTION STATEMENT A: Approved for public release; distriubution is unlimited.

13. SUPPLEMENTARY NOTES

14. ABSTRACT

15. SUBJECT TERMS

Tribology, Wear, Corrosion, Tribocorrosion, Stainless steel, Pitting, Passivation, Bearing

16. SECURITY CLASSIFICATION OF:			**17. LIMITATION OF ABSTRACT**	**18. NUMBER OF PAGES**	**19a. NAME OF RESPONSIBLE PERSON**
a. REPORT	**b. ABSTRACT**	**c. THIS PAGE**			Kathryn J. Wahl
Unclassified Unlimited	Unclassified Unlimited	Unclassified Unlimited	Unclassified Unlimited	15	**19b. TELEPHONE NUMBER** *(include area code)* (202) 767-5419

This page intentionally left blank.

CONTENTS

This page intentionally left blank.

IN SITU TRIBOCORROSION: UNCOVERING THE SCIENCE BEHIND COUPLED SURFACE DAMAGE PROCESSES

Kathryn J. Wahl[1], Derek J. Horton[2], Steven A. Policastro[2], Matthew J. Strom[2], Christopher R. So[1], Christopher N. Chervin[1], and Marybeth E. Parker[2]

[1]Code 6170, Surface Chemistry Branch
[2]Code 6130, Center for Corrosion Science and Engineering
Chemistry Division
Naval Research Laboratory
4555 Overlook Avenue, Washington, DC 20375

1. INTRODUCTION

Corrosion and wear damage are persistent, unavoidable problems that challenge Naval systems and are significant contributors to maintenance costs. When corrosion and wear are coupled, material lifetime can be severely decreased by the deleterious synergistic contributions of these processes to the protective oxide films. Subjecting corrosion resistant materials to friction and wear stresses in a corrosive environment can result in driving the surface from a protected state to actively corroding. What remains missing is the fundamental understanding of the mechanisms that operate at the junction between tribology and corrosion. We proposed to determine the physical mechanisms and reaction pathways that cause "tribocorrosion", and identify the fundamental science that drives the coupled surface chemistry and wear mechanics in corrosion resistant materials.

Material choices that separately meet standards for wear or corrosion resistance may, when exposed to service conditions, suffer from unexplained accelerated degradation. The speed and onset of the degraded performance can be astounding. We know little about this synergy between tribology and corrosion, and existing approaches do not adequately capture the underlying science. Today, the Navy treats corrosion and tribology resistance separately. To avoid corrosion, we often turn to high performance, passive alloys and cathodic protection. However, passive alloys and cathodic protection are not necessarily sufficient to protect surfaces from wear-induced corrosion. Furthermore, galvanic mismatches and even lubrication with seawater are unavoidable. This program worked to develop laboratory-scale science to determine the fundamental mechanisms governing tribocorrosion, and create models to predict how our materials will perform in the marine environment.

A schematic of the processes of interest in the coupled wear and corrosion problem is shown in Figure 1. Sliding stresses may remove the passivating oxide and cause other damage including plastic deformation of the underlying material and generation of wear debris.. Continually reforming the passive film will accelerate metal ion dissolution rates relative to passivated regions, while plastic deformation may cause a significant increase in dissolution rates by altering corrosion susceptibility regimes. Both processes may create conditions that overcome a critical rate threshold required to initiate self-propagating localized corrosion leading to substantial material loss. Similarly, corrosion may accelerate the wear processes by

Manuscript approved November 3, 2020.

generating weakened surfaces more susceptible to wear or increasing third-body formation that accelerate wear mechanisms.

Tribology and corrosion experiments typically assume full removal of the oxide, and current contributions are quantified through Faraday's law, $V = QM/(nF\rho)$, where Q represents the total charge transfer calculated by integrating the current transient, M the molar mass, n the mole averaged oxidation number, F the Faraday constant, and ρ the mass density of the alloy. Generally, the alloy is assumed to be passivating, with the background current dropping to a low level and only a small region of the wear track active as it re-passivates. Corrosion and wear related material losses are evaluated separately, and in combination. It is generally found that wear and corrosion combined cause increased material losses.

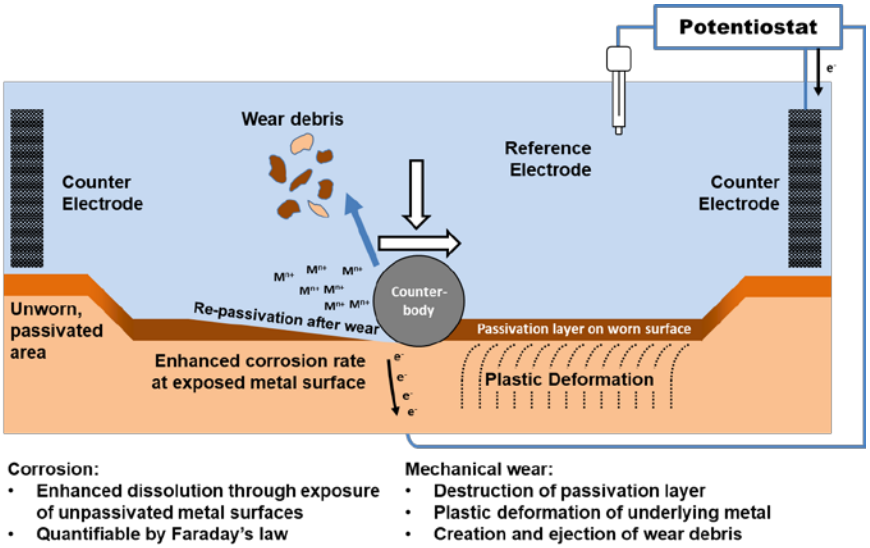

Figure 1 — Schematic of corrosion and mechanical wear processes (after [1])

2. EXPERIMENTAL APPROACH

In order to address the complex problem of the linkage between tribology and corrosion, new approaches are required to develop the science enabling us to explain and predict "tribocorrosion" behavior. We approached the problem by assembling an interdisciplinary research team with expertise in tribology and corrosion science and backgrounds in surface science, materials science, electrochemistry, and modeling. A significant challenge was to determine how the interaction between tribology and corrosion influences material removal and surface oxide degradation. Our proposed approach addressed three key aspects we believe necessary to address the science: (1) actively control the surface electrochemical state during measurements, (2) make measurements local to the active wear and repassivation process, and (3) determine how local materials interfaces, microstructures, and applied stresses contribute to tribocorrosion processes. To accomplish this, we developed experimental apparatus capable of electrochemistry and tribology measurements with state of the art approaches at scales ranging from macroscopic to nanometer (Figure 2).

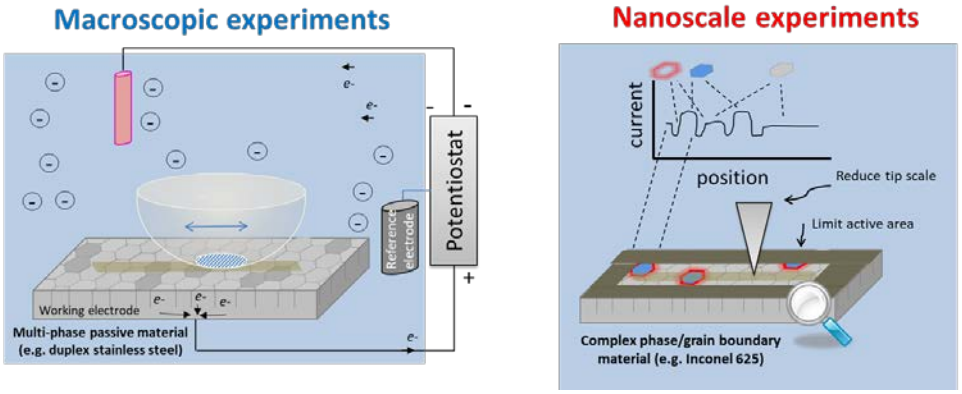

Fig. 2 — Tribocorrosion experimental concepts for macroscopic (left) and nanoscale (right) approaches

2.1 Macroscopic *in situ* tribocorrosion apparatus

We designed and constructed a reciprocating tribometer (Figure 3) using an open architecture setup with commercially available optics components on a rigid breadboard. Position of the load arm was controlled in height by a large lab jack mounted to the optical table, and lateral reciprocating kinematics with a linear motorized stage controlled by Labview software. The tribometer arm was mounted on a bearing allowing rotation about one (normal) axis and loads were applied through calibrated weights directly applied to the tribometer arm above the contact. A Wheatstone bridge configuration was used for lateral force measurements. We devised a rigid alumina mount for the counterbody. Alumina balls (1/4" diameter) were fixed to this with cyanoacrylate adhesive. Specimens were fixed to the bottom of the insulating polymer (polyvinylchloride) well and encircled by the counter electrode. The counter electrode material was platinum mesh and potential measurements were made using a saturated calomel reference electrode (SCE), with the sample serving as the working electrode. Before and during tribocorrosion testing, the sample was held at potentiostatic conditions maintained by a Gamry Reference 3000.

Sliding wear tests were conducted under potentiostatic conditions at either 100 mV_{SCE} or 600 mV_{SCE}, with samples allowed to passivate for at least 30 min before sliding. Wear tests were conducted at 1 mm/s sliding velocity with an amplitude of 10 mm. Tests were also run in deionized water (DI) to serve as a control environment with low ionic conductivity, no chloride and no applied potential.

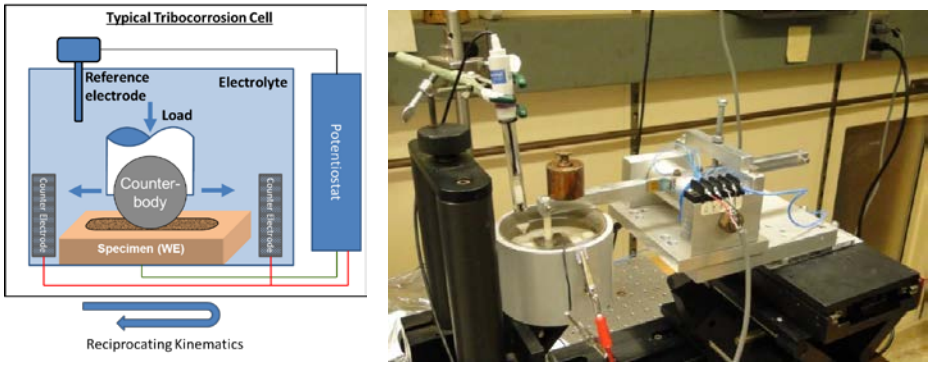

Fig. 3 — Macroscale tribocorrosion setup (left) and apparatus (right)

2.2 Nanoscale *in situ* tribocorrosion apparatus

We conducted nanoscale tribology experiments using an open configuration AFM (Nanoman, Veeco, Santa Barbara, CA) equipped with a tip holder made from polychlorotrifluoroethylene for fluid scanning (DECAFMCH-DD, Bruker, Camarillo, CA) and operated in contact mode with an external Nanoscope V controller (Bruker, Santa Barbara, CA). The sample was fixed to the bottom of a three-electrode electrochemical cell sized to fit under the AFM head. Standard calibration methods to determine cantilever spring constants, applied loads and tip geometry were employed. Experiments were performed primarily with commercially-sourced boron-doped polycrystalline diamond coated silicon cantilevers.

Samples were insulated using a photolithographic mask, with a small window between 100 x 100 μm to 10 x 10 μm window opened in selected regions identified by optical microscopy and SEM imaging. After polarizing the sample for 15 minutes, passive current densities were found to be similar to those measured for macroscopic experiments. Smaller windows were used to limit the total current on the order of 10 pA such that current changes resulting from nanoscale sliding contacts could be observed above the background.

Sliding electrochemical experiments were performed within the window regions while imaging continuously in contact mode. Scan rates were typically 2 Hz but was reduced for some experiments to 0.2 Hz to better resolve the electrochemical current data. A typical experiment involved collecting images at a given applied load, with each image taking about 60 s to collect, allowing the change in morphology, friction, and current to be monitored *in situ* as the surface was abraded. Images were either analyzed to obtain lateral force (friction force) data or current as a function of position, or averaged. Sequential image data was typically processed into videos to provide time-lapse views of the electrochemical and wear processes and aid in interpretation and presentation of the data.

2.3 Test materials

The primary material examined in this program was SAF 2507 (UNS 32750) duplex stainless steel. This material was selected as a good representative two-phase passivating chromium steel with large (100 micron scale) domains of ferrite and austenite phases. Through heat treating the steel at 800°C for 10, 30 and 60 minutes, we formed additional, potentially deleterious, secondary phases including secondary austenite, sigma, chi phases and chromium nitride inclusions (Figure 4). These samples were used to test the effects of sliding stresses on the materials as a whole and on separate phases using a spherical Al_2O_3 counterbody (macroscopic measurements) or a diamond or diamond-coated tip (nanoscale measurements). Experiments were performed in 0.6 M NaCl electrolyte was prepared using pure deionized (DI) water (18.2 MΩ·cm) and analytical-grade NaCl and was used at ambient temperature (25 °C) and aeration. Some reference experiments were performed in DI water.

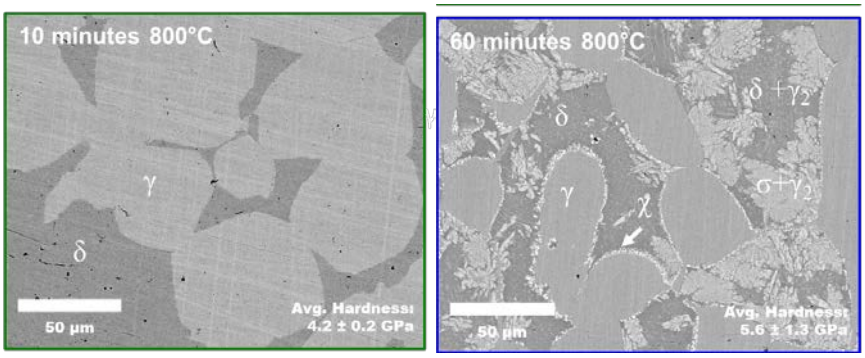

Figure 4 — Duplex stainless steel microstructure as received (left) and 60 min heat treated at 800C

After thermal processing surfaces were ground to remove thermally induced oxides, sectioned and an insulated wire was spot welded to the back side to permit electrical conductivity before the sample

was encased in epoxy. Samples were polished to 1 micron diamond and electroplating tape was used to reduce the exposed surface area and prevent crevice corrosion.

Scanning electron microscopy (SEM), energy dispersive x-ray spectroscopy (EDS), and X-ray diffraction (XRD) were used to identify phases and regions of interest and determine phase identity and compositions. Instrumented nanoindentation was used to assess the mechanical properties of individual phases. Potentiodynamic polarization experiments, sample passivation or depassivation, and tribocorrosion currents were controlled and monitored using a potentiostat. Wear track profiles were obtained with white light interferometry. Additional materials analysis was performed using Scanning Kelvin Probe Force Microscopy (SKPFM) and Conductive Probe Atomic Force Microscopy (CPAFM) to evaluate the work function and conductivity of the various phases found at the surface. Focused Ion Beam (FIB) milling was used to inspect subsurface structural changes to macroscopic wear tracks.

3. RESULTS

3.1 Macroscale tribocorrosion of duplex stainless steel

Heat treatments 2507 of duplex stainless steel resulted in the formation of deleterious phases including secondary austenite and sigma phase, as well as chromium nitride inclusions. Materials properties for the as received and heat treated steels were examined. The corrosion performance was not appreciably altered by the heat treatments and presence of secondary phases (Figure 5). The materials changes manipulated the overall structure of the alloy, resulting in chemical partitioning of protective chromium around the new phases particularly nitrides. Despite this, the variations in chromium concentration were not sufficient to induce a breakdown of passivity, even at high applied potentials. Hardness was increased after heat treatments, which was attributed to localized increases in hardness from the sigma phase regions.

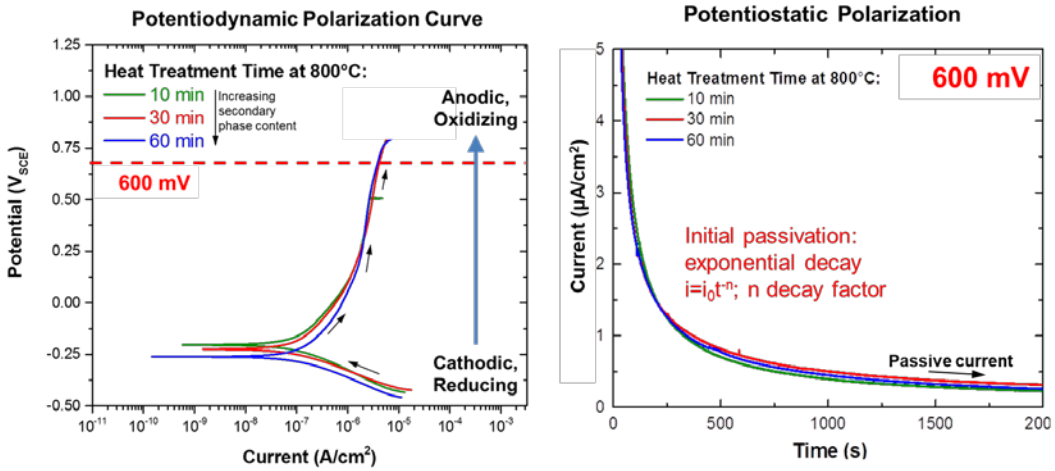

Figure 5 — Heat treatments of the stainless steel and formation of secondary phases did not significantly impact the polarization curves (left) or repassivation behavior (right) prior to sliding wear

Sliding experiments against the three sample treatments (as received, 30 and 60 minutes at 800°C) were performed. In NaCl solutions, friction data was similar for all experiments, with relatively high values ranging between 0.38 to 0.45, after an initial run-in period where friction rose to above 0.5. Friction was generally similar between 100 and 600 mV conditions. Friction in DI water was somewhat higher and less stable, between 0.5-0.6. For samples tested at 100 mV_{SCE}, once sliding started the

corrosion current was stable between 2 and 3.5 mA. Once sliding stopped, the worn sample surfaces quickly repassivated to corrosion currents close to the initial passivation level. At 600 mV, the samples behaved quite differently. Short heat treatment (10 min) to 800°C showed similar behavior to the 100 mV tests, but for the 30 minute heat treated samples the current was unstable and increasing during sliding, and the upward trend accelerated after sliding was ceased and the surface did not repassivate; additional deleterious phase precipitation time at 800°C accelerated the poor current performance and again prevented repassivation after sliding.

Analysis of the surfaces after sliding using optical microscopy and SEM revealed the presence of pits on the surface in and near the wear tracks (Figure 6). Sectioning the wear tracks by FIB revealed a network of interpenetrating voids under the wear tracks, demonstrating substantial mass loss in these regions. Damaged regions were primarily associated with secondary austenite and sigma phases. Predicted mass loss from the current measurements using Faraday's law exceeded measured mass loss from the surfaces of wear tracks. However, this can be reconciled by considering that the material loss penetrates below the surface of the wear track. This occurred because the network formed by the sigma phase and secondary austenite is lamellar and creates pathways for electrolyte to penetrate under the surface as one phase is preferentially corroded. This process likely starts through local depassivation in the wear track in a region more susceptible to corrosion, such as the Cr-depleted secondary austenite. Once initiated, we speculated that the pitting is driven by purely corrosive pit growth phenomena such as local pH increases. This behavior makes the standard synergistic tribocorrosion model [1] an inappropriate model to apply to this system, as it was largely developed for passivating alloys not exhibiting any other corrosion related processes such as pitting.

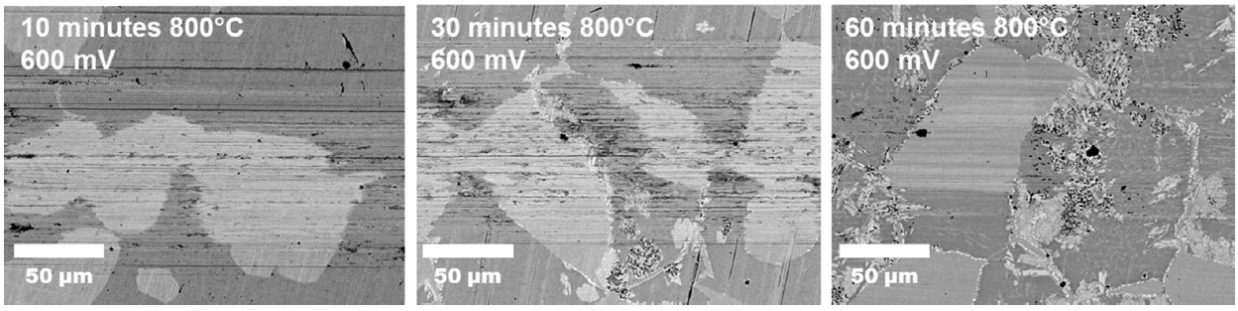

Figure 6 — SEM images (backscattered electron z-contrast) of wear track surface analysis for sliding experiments in 0.6M NaCl at 600 mV. Dark features are pits.

In summary, we found that the formation of secondary austenite, sigma, chi, and other tertiary phases through heat treatment at 800°C produced no notable differences in the corrosion behavior of 2507 at low and high anodic potential measured in the absence of sliding contact. Sliding tribocorrosion experiments revealed that the presence of sigma and other secondary phases influenced the repassivation behavior, with longer heat treatment times resulting in a steadily increasing pitting corrosion current that continued to climb even after sliding stopped. Sliding stresses and the resulting surface damage disrupted the passivity in microstructural regions containing lower chromium content, as this correlated to pitting corrosion at and below the surface at the secondary austenite phase, both within and in regions near to the wear track. This work is presented in detail in [2].

3.2 Nanoscale electrochemical measurements of sliding against duplex stainless steel

Results from the macroscale sliding experiments were surprising and caused us to wonder what specific aspects of the duplex stainless steel material properties drove the susceptibility to localized corrosion after heat treatments. We pursued the possibility of exploring initiation and propagation of the

tribocorrosion damage, in individual phases or specific phase interfaces at scales where the sliding stresses were localized by reducing the size of the sliding contact to below the dimensional size of the phase domains. This was possible through combining liquid cell AFM with tribology and electrochemistry approaches and restricting the exposed surface area using photolithography. This was essential to the success of the measurement as it reduced the background corrosion current to pA levels allowing us to measure the current arising from nanometer scale contacts subjected to sliding stresses and damage.

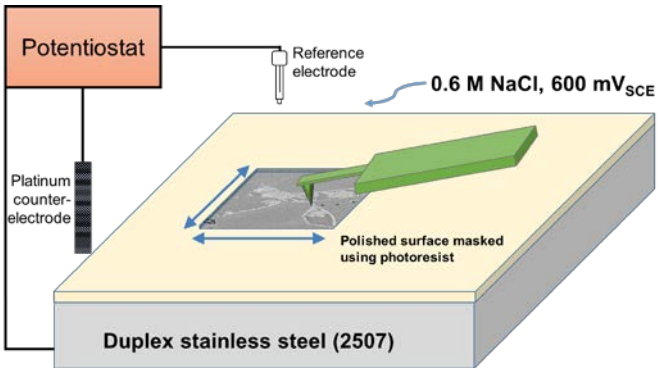

Figure 7 — AFM electrochemical setup for tribology measurements. Experiments were performed in 0.6M NaCl at various potentials. The exposed window allowed reduced background currents and locating regions of interest with multiple analytical techniques.

We were able to find and identify the phase of each grain in the experiments by combining scanning electron microscopy (SEM) and EDX composition mapping of the exposed window with the features we observed in the topographic imaging by AFM. The sigma phase regions are somewhat harder than the rest of the matrix, which results in slightly elevated grains from differential polishing effects. By comparing the SEM and EDX imaging with the AFM images regions such as the one in Figure 8, left were selected that had a mixture of phases. (). An example of the surface topography after wear by the diamond AFM tip is shown in Figure 8, center. The color scale indicates depth, with white/light blue regions showing the original surface polish with slightly raised sigma phase regions, and darker blue, green and red regions showing significant wear. The wear is localized primarily to secondary austenite and some ferrite regions. Figure 8, right also shows that the current measured in the electrochemical during the wear process is spatially correlated with the wear loss. There is a tremendously rich scientific opportunity shown here. In our experiments, we worked to identify the susceptible phases, the nature and magnitudes of the sliding stresses required to initiate the localized material removal, and the magnitude and relationship of the current in the electrochemical cell to the material removal process.

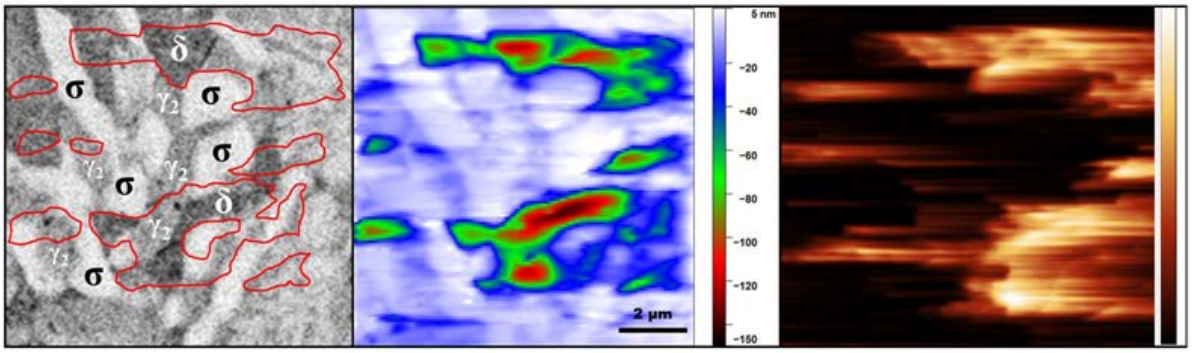

Figure 8 — Backscattered SEM image showing z-contrast and identification of phases (left), worn surface topography from AFM experiment (center), and image created by summing current in the electrochemical cell relative to tip position during sliding wear (right, arbitrary units with brighter regions having higher current)

We were able to quantitatively measure material loss rates as a function of sliding stress, sliding cycles, and phase (Figure 9). Surprisingly, we found that at lower stresses sliding wear was initiated at chromium nitride inclusions (Figure 9, left). Ultimately, the wear rates in these regions dropped, and wear in the surrounding austenite and sometimes other phases accelerated. Wear rates were fairly linear with respect to sliding passes and were typically an order of magnitude higher in the secondary austenite regions than in the sigma phase regions, when wear was observed. There was some evidence that tip sliding direction and the phase to phase transition, i.e. the phase most recently contacted, may influence the sliding-induced wear under these conditions. We argued that was likely a result of the specific local chemistry of the electrochemical region surrounding the sliding AFM tip, which can vary depending on what phase is subjected to wear. This could account for the observation that the sliding tip has contacted before contributed to the material removal process.

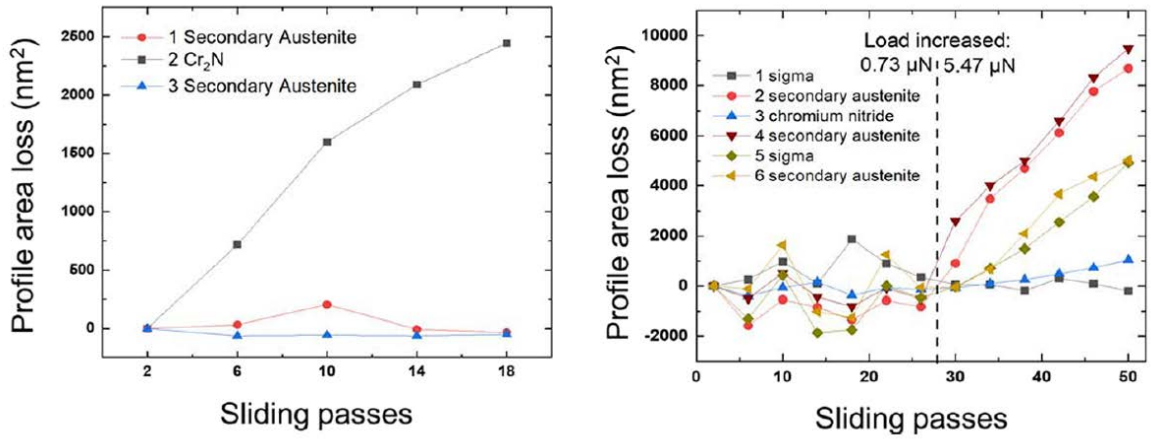

Figure 9 — Wear rates as a function of sliding cycles and phase (left) and as a function of load and sliding cycles (right)

The initial material loss and propagation of electrochemical wear solely from chromium nitrides (Figure 10, left/center) is surprising, as these inclusions ultimately resist wear under extended sliding, in contrast to surrounding secondary austenite and ferrite. The nobility of Cr_2N relative to the other phases (Figure 10, right) suggest that it should be less susceptible to local electrochemical attack. Why the nitrides were the first phase to wear under low load, electrochemically active conditions, but not inert conditions, is not yet understood.

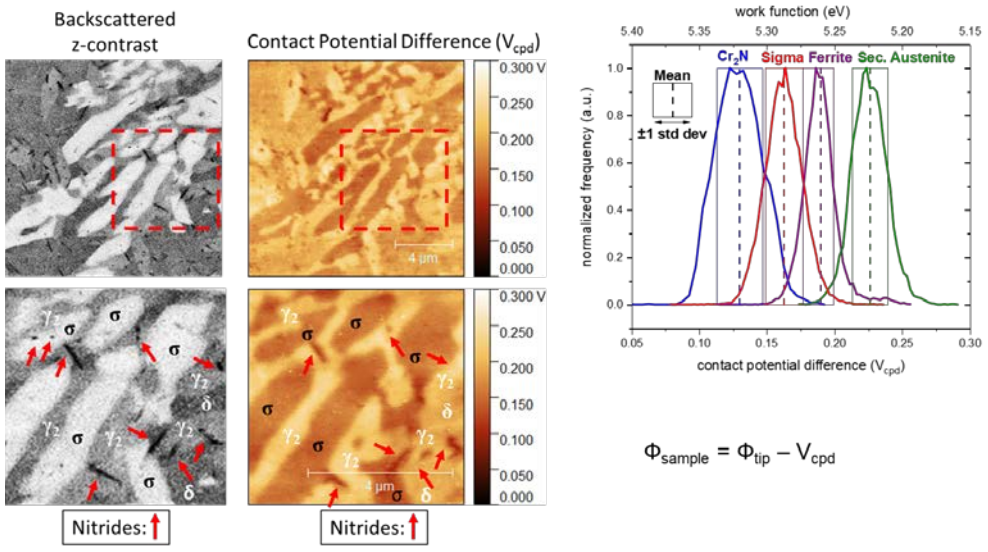

Figure 10—SEM (left greyscale images) and AFM topography (middle images) images of the initial surface wear at low contact stress showing electrochemical wear initiation at chrome nitride inclusions. At right, the work function for each phase measured by SKPFM showing the relative nobility of the phases, with chrome nitrides being most noble of the phases.

As noted above and shown in Figure 8, we found that the localized material loss corresponded to current generation. The current was linearly correlated with material loss, although the magnitude did not. Additional experiments to determine the nature of the currents with potentiostatic polarization curves revealed that the boron doped diamond tip in contact with the specimen during sliding wear provide an electrical path to the Pt clip. This electrical path is mediated by the resistivity of the metal oxide layer which may change as layers are removed during sliding, resulting in heightened sensitivity to the surface changes and electrochemical processes in the cell during wear. This work is presented in full in reference [3].

4. MODELING

We have worked to develop another modification to the nanoscale sliding experiment to remove any conductivity contributions to the measurements by using single crystal diamond tips on the AFM cantilevers. These measurements clarify the current magnitudes to the expected range for oxide repassivation, and also continue to demonstrate that the fundamental relationship between stress and measured current during sliding is non-linear. How the effects of oxide removal, plastic deformation and applied stress combine to manipulate the measured currents is as yet unknown. The form of the nanoscale data is consistent with an Arrhenius model, which has been observed for a number of other nanoscale sliding processes where thermodynamics can play a role. To this end, we have worked to examine the relationship between measured current and applied contact stress during electrochemical wear in nanoscale sliding contacts. Our evidence points to a partial removal of oxide, complicating the projections of current from the process. This again raises the issue that the materials science is more complicated than allowed by the standard assumptions made by tribocorrosion community, which assumes full removal of the surface oxide. We are completing a model which takes these oxide removal processes into account. We are combining these two models to account for the effects of applied stress and resultant wear and oxide regrowth to predict the form of the data observed in the experiments.

5. CONCLUSIONS

We have successfully performed macro- and nanoscale measurements of tribocorrosion processes on a model duplex stainless steel. We found that sliding stresses significantly impacted corrosion susceptibilities of the surfaces studied, and initiated pitting corrosion of selected phases at both scales. Heat treatments produced deleterious secondary phases that were more susceptible to corrosion-related wear acceleration than surrounding materials; the most susceptible phases were depleted in chromium relative to the parent steel phases. Nanoscale experiments showed similar trends, with the added resolution revealing that the chromium nitrides played a role in the initial wear response in electrochemically active conditions, before wear of the less noble and more susceptible phases proceeded. We are working to complete modeling of these processes with advanced approaches accounting for partial, rather than complete, removal of oxides from surfaces during wear. This is important because normal wear of surfaces in engineered systems does not proceed through the high damage rates found in the laboratory experiments. That contribution would tie together the observations and underlying mechanisms allowing us to predict fundamental wear phenomena under tribocorrosion conditions.

REFERENCES

1. S. Mischler, S.Debaud, D.Landolt, 1998, “Wear-accelerated corrosion of passive metals in tribocorrosion systems,” J. Electrochem. Soc. 145(3), 750–758.

2. J. M. Shockley, D.J. Horton and K.J. Wahl, 2017, Effect of aging of 2507 super duplex stainless steel on sliding tribocorrosion in chloride solution, Wear 380-38, 251–259.

3. J. M. Shockley, C.R. So, M.J. Strom, R.C.Y. Auyeung, D.J. Horton and K.J. Wahl, 2020, “Direct Observation of Corrosive Wear by *In Situ* Scanning Probe Microscopy,” ACS Appl. Mat. Inter. 12, 23543-23553.

6. PAPERS AND CONTRIBUTED PRESENTATIONS

6.1 Papers

1) J. Michael Shockley, D.J. Horton, and K.J. Wahl, 2017, "Effect of Aging of 2507 Super Duplex Stainless Steel on Sliding Tribocorrosion in Chloride Solution," Wear 380-381, 251-259.
2) Jacobs, T.D.B.; Greiner, C.; Wahl, K.J.; Carpick, R.W., 2019, "Insights into tribology from *in situ* nanoscale experiments," MRS Bulletin 44, 478-486.
3) J. M. Shockley, C. R. So, M. J. Strom, D. J. Horton, and K. J. Wahl, 2020, "Direct observation of corrosive wear by *in situ* scanning probe microscopy," ACS Appl. Mat. Inter. 12, 23543-23553.

6.2 Talks

1) D.J. Horton , S. Policastro, J.M. Shockley, K.J. Wahl, "*In situ* Tribocorrosion," NRL Branch Review, 18 February 2016.
2) J. Michael Shockley, D.J Horton and K.J. Wahl, "Tribocorrosion of Super Duplex Stainless Steel," poster, Tribology Gordon Graduate Research Seminar, Bates College, Lewiston, Maine, 25-26 June 2016.
3) J. Michael Shockley, D.J Horton and K.J. Wahl, "Tribocorrosion of Super Duplex Stainless Steel," poster, ONR Corrosion in 4D MURI Review, University of Virginia, Charlottesville, VA, 30 June-1 July 2016.
4) J. Michael Shockley, D.J Horton and K.J. Wahl, "Tribocorrosion of Super Duplex Stainless Steel," poster, Corrosion - Aqueous Gordon Conference, Colby Sawyer College, New London, NH, 10-15 July 2016.
5) K.J. Wahl, (**INVITED**) "*In situ* approaches to understand adhesion, friction, and wear in the marine environment," Department of Mechanical Engineering Seminar, University of Illinois at Urbana Champaign, 13 September 2016.
6) J. M. Shockley, D.J. Horton and K.J. Wahl, "Studying the Tribocorrosion Behavior of Duplex Stainless Steels in Chloride Media Using Spatially Resolved Friction and Electrochemical Measurement," Society of Tribologists and Lubrication Engineers Tribology Frontiers Conference, Chicago, IL, 13-15 November 2016.
7) K.J. Wahl, J.M. Shockley, C.R. So, D.J. Horton, S.A. Policastro, A. Carney, "*In Situ* Tribocorrosion: Uncovering the Science Behind Coupled Surface Damage Processes", NRL 6.1 Branch Review, Washington, DC, 8 February 2017.
8) J.M. Shockley, D.J. Horton, S. Policastro, C.R. So and K.J. Wahl, "Linking microstructure to wear-induced pitting corrosion in aged 2507 super duplex stainless steel," American Chemical Society Annual Meeting, San Francisco, CA, 2-6 April 2017.
9) J.M. Shockley, D.J. Horton, S. Policastro, C.R. So and K.J. Wahl, "Linking microstructure to wear-induced pitting corrosion in aged 2507 super duplex stainless steel," Society of Tribologists and Lubrication Engineers Annual Meeting, Atlanta, GA, 21-25 May 2017.
10) J.M. Shockley, D.J. Horton, C.R. So and K.J. Wahl, "Linking microstructure to wear-induced pitting corrosion in aged 2507 super duplex stainless steel," International Conference on Trends in Nanotribology 2017, Trieste, ITALY, 26-30 June 2017.
11) J.M. Shockley, C.R. So, D.J. Horton, S.A. Policastro, and K.J. Wahl, "Studying tribocorrosion mechanisms of aged 2507 super duplex stainless steel by scanning probe microscopy," 232nd Electrochemical Society (ECS) Meeting, National Harbor, MD, 1-5 October 2017.
12) J.M. Shockley, D.J. Horton, C.R. So and K.J. Wahl, "Linking microstructure to wear-induced pitting corrosion in aged 2507 super duplex stainless steel," Nanotribology Meeting, Goa, INDIA, 8-12 January 2018 (poster).
13) J.M. Shockley, C.So, D.J. Horton, K.J. Wahl, Scanning probe tribocorrosion of aged 2507 duplex stainless steel. 73rd STLE Annual Meeting & Exhibition Minneapolis, MN, May 21, 2018.

14) **INVITED** J.M. Shockley, C.R. So, M. J. Strom, D.J. Horton and K.J. Wahl, "Tribocorrosion of Passivating Alloys: Initiation and Propagation in Large and Small Contacts," Tribology Gordon Research Conference, South Hadley MA, 24-29 June 2018
15) K.J. Wahl, J.M. Shockley, C.R. So, D.J. Horton, S. Policastro, M. Strom, "In situ tribocorrosion: Uncovering the science behind coupled surface damage processes," Chemistry Division External Review, NRL, 25 June 2018.
16) **INVITED** J.M. Shockley, C.R. So, M. J. Strom, D.J. Horton and K.J. Wahl, "Quantitative tribocorrosion of nanocontacts to steel," Nanotribology Meeting in Potsdam, Germany, 2-4 October 2018
17) (**INVITED**) J.M. Shockley, C.R. So, M.J. Strom, D.J. Horton, and K.J. Wahl "Quantitative tribocorrosion of nanocontacts to steel" Colloquium, Department of Mechanical Engineering, Texas A&M University, College Station, Texas, 31 October 2018
18) J.M. Shockley, C.R. So, D.J. Horton, M. Strom, and K.J. Wahl, "Scanning probe tribocorrosion of aged 2507 super duplex stainless steel," EuroCorr 2018 (Annual Meeting of the European Federation of Corrosion), Cracow, Poland, 9-13 September 2018.
19) Parker M. E., Shockley, J. M.; Storm, M. J.; So, C. R.; Wahl, K. J.; Horton, D. J. Impact of Potential on the Tribocorrosion Behavior of Duplex Stainless Steels. Presented at NACE Corrosion 2019, Nashville, TN, 25 March 2019.
20) Parker, M.E.; Shockley, J. M.; So, C. R.; Strom, M. J.; Wahl, K. J.; Horton, D.J. Impact of Potential on the Tribocorrosion Behavior and Electrochemical Response During Scanning Probe Tribology of Duplex Stainless Steels, French Defense Exchange Agreement Meeting, NRL-Key West, 20 June 2019.
21) Birnbaum, A.; Ryou, H.; Steuben, J.; Iliopoulos, A.; Wahl, K.J., Nested Size Effects Observed in Nanoindentation Studies of Additively Manufactured 316L Stainless Steel. Solid Freeform Fabrication Conference, Austin TX, 12-14 August 2019.
22) Ryou, H.; Wahl, K.J.; Gorzkowski, E.P.; Michopoulos, J.G.; Birnbaum, A.J., Indentation Size Effect in Additively Manufactured 316L Stainless Steel. Materials Science and Technology 2019, Portland, OR, 29 September – 3 October 2019 (poster).
23) (**INVITED**) Shockley, J.M.; So, C.R.; Strom, M.J.; Horton, D.J.; Wahl, K.J., Quantitative tribocorrosion of nanocontacts to steel. International Nanotribology Forum (in memoriam Jacob Israelachvili), Chiang Rai, Thailand, 13-17 January 2020.
24) M.E. Parker, D.J. Horton, K.J. Wahl, "Impact of Sliding Wear on the Pitting Behavior of Duplex Stainless Steels," Virtual Eurocorr, 9 September 2020.